Shape-morphing carbon fiber composite using electrochemical actuation

Wilhelm Johannisson[a], Ross Harnden[a], Dan Zenkert[a,1], and Göran Lindbergh[b]

[a]Department of Aeronautical and Vehicle Engineering, KTH Royal Institute of Technology, SE-100 44 Stockholm, Sweden; and [b]Department of Chemical Engineering, KTH Royal Institute of Technology, SE-100 44 Stockholm, Sweden

Edited by David A. Weitz, Harvard University, Cambridge, MA, and approved February 28, 2020 (received for review December 5, 2019)

Structures that are capable of changing shape can increase efficiency in many applications, but are often heavy and maintenance intensive. To reduce the mass and mechanical complexity solid-state morphing materials are desirable but are typically nonstructural and problematic to control. Here we present an electrically controlled solid-state morphing composite material that is lightweight and has a stiffness higher than aluminum. It is capable of producing large deformations and holding them with no additional power, albeit at low rates. The material is manufactured from commercial carbon fibers and a structural battery electrolyte, and uses lithium-ion insertion to produce shape changes at low voltages. A proof-of-concept material in a cantilever setup is used to show morphing, and analytical modeling shows good correlation with experimental observations. The concept presented shows considerable promise and paves the way for stiff, solid-state morphing materials.

solid state | zero-power hold | structural composites | high stiffness | electrically controlled

Structures that can change their shape by morphing between two or more stable geometries are advantageous in a wide variety of applications such as aerospace, renewables, and robotics: for example, trimming of aerodynamic surfaces for steady-state conditions in aircraft and wind turbines, and deployment of satellite booms. The problem with current state-of-the-art morphing technologies is that they use systems of heavy mechanical motors, hydraulic/pneumatic pumps, or solenoids to create shape changes. These systems add parasitic weight, and are mechanically complex, adding to maintenance costs. One way to reduce the mechanical complexity is to use solid-state morphing materials.

A wide range of materials have been shown to exhibit controllable solid-state shape-changing capabilities. Typically, actuation devices can be characterized in terms of actuation force, strain, stiffness, operating frequency, and efficiency, among other parameters (1). Piezoelectric materials have proven to offer high operating frequencies and reliability; however, they are most often nonstructural, and rely on high operating voltages in order to deliver high actuation forces (2–4). Pseudocapacitive actuation materials are capable of delivering high actuation frequencies and high actuation strains at low operating voltages (5–12); however, they are most often reliant on liquid electrolytes for operation, which discounts their use as structural components. Shape-memory alloys are good actuation materials, and have been demonstrated in many applications in aerospace (13). Their use is however limited to applications where shape changes can be triggered by changes in temperature or pressure. All of the above also rely on a constant supply of power in order to maintain deformations, which limits their use in energy-sensitive applications. Intercalation-based actuation can offer high actuation forces at low voltages, as well as inherently having the ability to maintain deformations without a constant supply of power, known as a zero-power hold. However, intercalation actuation devices are limited by low operating frequency and have relied on liquid electrolytes to allow ion transport between electrodes which has prevented any practical use in structural components (14–17).

In order for morphing structures to become more widely used—and hence enable more efficient design—there is a need for a morphable solid-state material that is lightweight and stiff, exhibits a zero-power hold, and is easy to control and integrate into existing structures. A material that can fulfill these needs is still to be conceived.

This article demonstrates a proof-of-concept for a stiff, morphable solid-state composite material. It is made from commercial carbon fibers and a structural battery electrolyte (SBE). By combining these elements we show that is it possible to form a low-density material with a stiffness higher than that of aluminum, that is morphable at voltages up to 1.5 V, exhibits an inherent zero-power hold, and can produce large deformations and high gravimetric actuation energies. The morphing material is characterized mechanically, and its behavior agrees well with modeling predictions.

Carbon fibers are a good candidate for creating multifunctional materials, having some of the best strength and stiffness to weight ratios of any commercially available material, and being electrically conductive. The microstructure of polyacrylonitrile-based carbon fibers is turbostratic and consists of graphitic and amorphous carbon (18). This structure is amenable to lithium (Li) storage, allowing carbon fibers to be used as negative electrodes in Li-ion batteries, with good electrochemical efficiency (19, 20). Graphite expands linearly by as much as 4.2% when Li is inserted into its microstructure through a well-known process known as intercalation (16). There is, however, no consensus on

Significance

Structures that can change their shape are advantageous in a wide variety of applications such as aerospace, renewables, and robotics. The problem with current shape-changing technologies is that they are either heavy, lack mechanical stiffness, or are hard to control. This paper demonstrates a shape-changing carbon fiber composite material, which is lightweight, has a stiffness higher than aluminum, and is electrically controlled. Future applications for this material could include trimming of aerodynamic surfaces for steady-state conditions in aircraft and wind turbines, and deployment of satellite booms.

Author contributions: W.J., R.H., D.Z., and G.L. designed research; W.J., R.H., and D.Z. performed research; W.J., R.H., and D.Z. contributed new reagents/analytic tools; W.J., R.H., D.Z., and G.L. analyzed data; and W.J., R.H., D.Z., and G.L. wrote the paper.

The authors declare no competing interest.

This article is a PNAS Direct Submission.

Data deposition: The raw data for Figs. 3 and 4 and *SI Appendix*, Figs. S1 and S2 and Tables S1 and S2 are available in Mendeley Data (https://doi.org/10.17632/4zky6h8w3v.1).

[1]To whom correspondence may be addressed. Email: danz@kth.se.

This article contains supporting information online at https://www.pnas.org/lookup/suppl/doi:10.1073/pnas.1921132117/-/DCSupplemental.

First published March 25, 2020.

how Li inserts into amorphous carbon (21). Measurements on carbon fibers have shown that they expand along their fiber direction by up to 1% when inserted with Li (22). This expansion is reversible and approximately linear with the state of charge, which corresponds to the amount of inserted Li in the carbon fibers. The electrochemical insertion reaction requires low electrical potentials. The fibers will remain expanded when no current is running, thus exhibiting a zero-power hold. Such expansions have been proposed as a possible way to create linear actuation using liquid electrolytes (22). Additionally, it has been shown that even after 1,000 repeated Li insertion cycles the mechanical properties of carbon fibers remain largely unaffected (23). However, to realize a solid-state morphing material, a matrix is required that can both transfer mechanical load between fibers and conduct ions which enables the electrochemical functionality of the carbon fibers.

Solid electrolytes are being developed in order to improve conductivity, safety, and stability of Li batteries (24). However, these are structurally low performing and cannot be used to transfer mechanical load. An SBE has been developed recently for structural battery applications that adheres to carbon fibers, transfers mechanical load, conducts Li ions, and allows Li insertion into carbon fibers (25–27). The SBE consists of two phases: a structural polymer backbone for mechanical load transfer and a liquid for ion conductivity, forming an interpenetrating and percolating network on a nanoscale (Fig. 1*A*). The properties can be tailored by choice of SBE constituents and curing process. The SBE therefore fulfills the necessary multifunctional matrix requirements for realizing a solid-state morphing material.

The morphing material presented here is formed from two Li-activated carbon fiber layers, electrically insulated from one another by a commercial ceramic separator layer and embedded in the SBE to form a structural composite laminate (Fig. 1*B*). By applying an electrical current Li ions are transferred through the SBE from one carbon fiber layer to the other, causing the discharging layer to contract, while the charging layer expands, morphing the entire laminate in a bending motion (Fig. 1*C*). The morphing mechanism is thus provided by the load-carrying material itself, forming a truly multifunctional material that adds little to no parasitic mass to a structure and is electrically controlled.

Results

Preparation and Characterization. The composite material is fabricated using two layers of spread unidirectional carbon fibers separated by a layer of ceramic Li-ion battery separator material

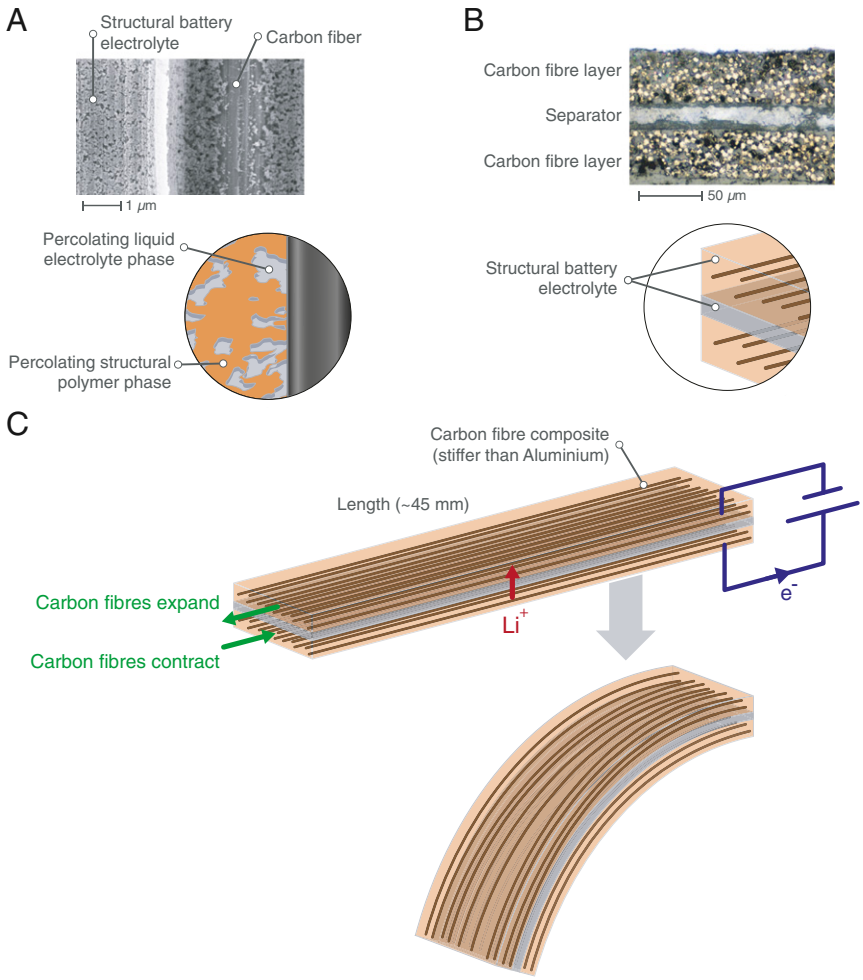

Fig. 1. Solid-state carbon fiber composite morphing material in a cantilever setup. (*A*) SEM image and schematic of carbon fiber and SBE. (*B*) The composite material consists of two unidirectional Li-activated carbon fiber layers, and one ceramic-based Li-ion battery separator layer. All three layers are embedded in an SBE. A representative cross-section of the material captured using a light microscope is also shown. (*C*) Li ions are discharged from one carbon fiber layer to the other by application of a current, causing the discharging layer to contract in the fiber direction, and the charging layer to expand. This creates an overall bending deformation.

(Fig. 2*A*). Current collectors are attached to the two carbon fiber layers for electrical connection. The three layers are assembled on a flat mold and vacuum infused with SBE and subsequently heat cured (Fig. 2*B*). The resulting composite material (Fig. 2*C*) has an approximate density of 1,600 kgm^{-3}. The carbon fiber layers are activated as follows: the cured composite material is placed into a pouch cell bag with a layer of Li metal foil on either side, separated from the carbon fiber layers by a glass fiber paper, soaked in liquid electrolyte, and vacuum sealed in the pouch cell (Fig. 2*D*). The two carbon fiber layers are then fully charged/discharged at a low constant current density for several cycles before being left at 50% state of charge (see *SI Appendix*, Fig. S1 for charge/discharge profiles). This activation partially expands the carbon fiber layers by an equal amount. The cell was then disassembled, the laminate taken out and sealed with a thin, low-density polyethylene film to prevent solvent evaporation. The laminate was then placed in a custom-made bending rig forming a cantilever, with morphing controlled by a potentiostat as a current source (Fig. 2*E*). All morphing experiments were carried out in a dry argon atmosphere.

Layer thicknesses were obtained by measuring cross-sections using a light microscope, giving carbon fiber layer thicknesses of ∼50 μm, and a separator layer thickness of ∼20 μm (*SI Appendix*, Table S1). An example cross-section is shown in Fig. 1*B*. Theoretical predictions and material testing results in a homogenized longitudinal in-plane modulus of the laminate, including the separator layer, of over 100 GPa, higher than the 69 GPa of aluminum (*SI Appendix*, Table S2). This is three orders of magnitude higher than the stiffness reported for similar morphing materials elsewhere in the literature (15, 16, 28).

Morphing Performance. The morphing experiments were carried out by applying a constant current between the two carbon fiber layers using voltage cutoff limits of −1.5 and 1.5 V. This creates a bending deformation in the composite material due to the transfer of Li, as one carbon fiber layer charges and expands, while the other discharges and contracts. The morphing was captured using a video camera, and the resulting films were processed using image tracking and digital image correlation to calculate the displacements. Fig. 3 shows one full upward and downward stroke at a current density of 14.5 mAg^{-1}, with regard to the mass of one of the carbon fiber layers. For a cantilever length of 48 mm this resulted in a maximum tip displacement of ∼35 mm, with one full stroke to either the upward or downward positions taking just over 5 h.

Movie S1 shows a time-lapse film of the morphing of a cantilever at two different current densities. The time lapse is recorded such that 1 s of video corresponds to 15 min in real time. Firstly, a downward stroke is shown followed by a return stroke to the neutral position. A similar movement is then shown beginning with an upward stroke. These are carried out at a current density of 44.2 mAg^{-1} and take ∼20 min per stroke. Secondly, a new stroke is performed using a lower current density (14.5 mAg^{-1}) which produces larger displacements due to a higher charge transfer, albeit with a time per stroke of just over 5 h, snapshots of which are shown in Fig. 3. A 1-h period of no current is applied between each stroke to allow any Li concentration gradients to relax and additionally shows that the morphing composite material exhibits a zero-power hold. With an open circuit no currents are running and the potential difference between the carbon fiber layers is maintained, producing the zero-power hold.

Morphing Predictions. The morphing deformation is created by one carbon fiber layer expanding while the other contracts, corresponding to strains $\varepsilon^{+}/\varepsilon^{-}$, respectively. These strains, together with layer thicknesses and elastic moduli, are used as inputs to an analytical model based on beam theory, which is analogous to the analysis of a bimetal thermostat (29).

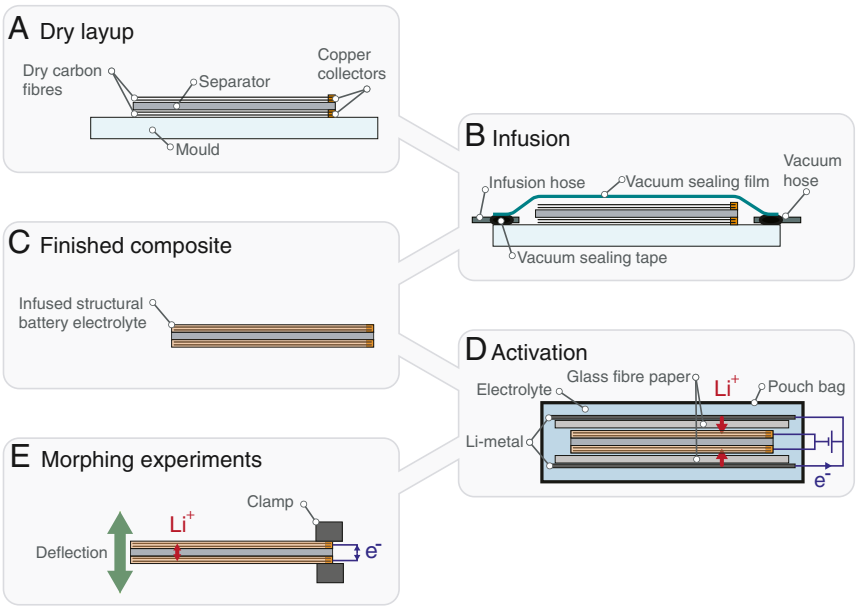

Fig. 2. Fabrication process for the carbon fiber composite morphing material. (*A*) Two unidirectional carbon fiber layers and one ceramic separator layer are laid up on a mold. Copper current collectors are attached to the carbon fiber layers. (*B*) The layup is sealed with a vacuum-sealing film and tape, and the SBE is infused into the three layers under vacuum, before being heat cured for 45 min at 90 °C. (*C*) The cured three-layer composite material, with a density of ∼1,600 kgm^{-3}, is ready for the activation process. (*D*) Two layers of Li metal foil are used as a source of Li ions and are placed on either side of the composite material, separated by layers of glass fiber paper soaked with liquid electrolyte. This is then sealed under vacuum inside a pouch bag. A current is applied (18.6 mAg−1) between the Li foil and the carbon fibers and the carbon fiber layers are charged/discharged several times before being left charged at 50% state of charge. (*E*) The composite material is removed from the pouch bag and clamped to form a cantilever. A current is applied between the two carbon fiber layers, charging/discharging the layers between −1.5 and 1.5 V causing the cantilever to bend.

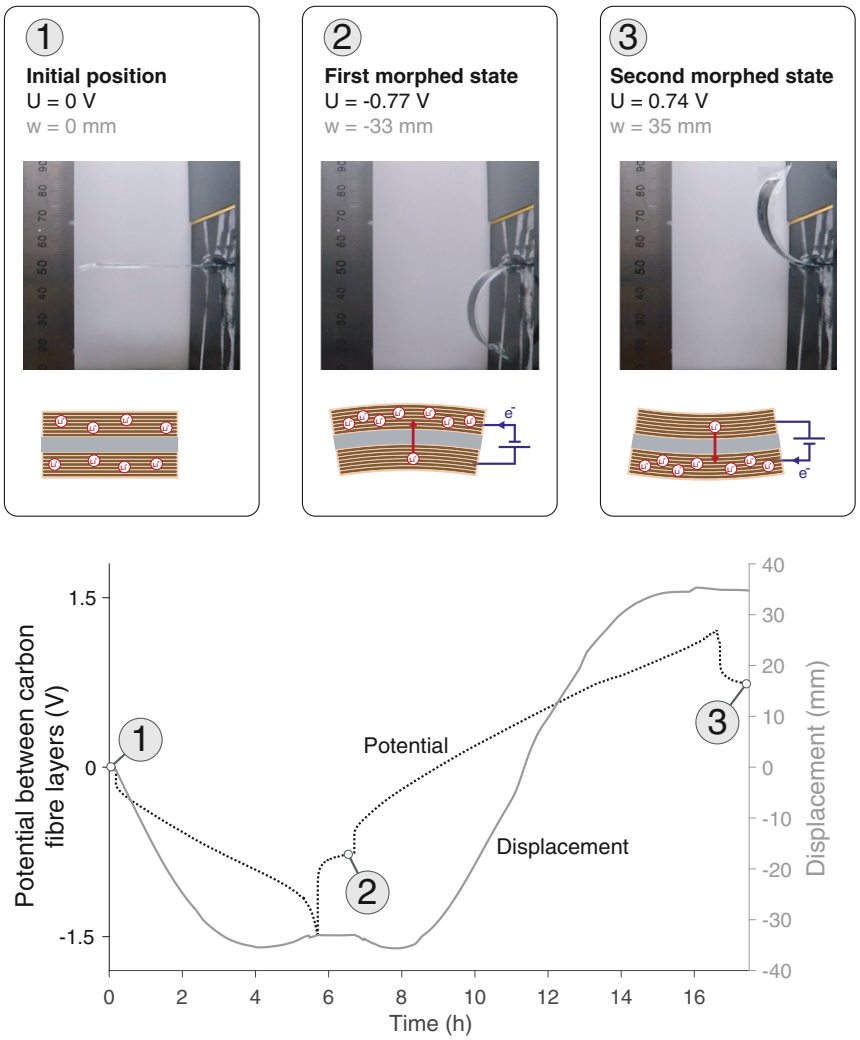

Fig. 3. Experiment showing the morphing carbon fiber composite material in a cantilever setup. A current is applied between the carbon fiber layers with cutoff voltages of −1.5 and 1.5 V. This causes Li to transfer from one carbon fiber layer to the other. The charging carbon fiber expands in the fiber direction as it reaches a higher state of charge, while the carbon fiber layer that is discharging contracts, creating a bending deformation. Potential difference between the carbon fiber layers and cantilever tip displacement are shown as functions of time. Images showing displacements of the morphing material are also shown. For a cantilever length of 48 mm a maximum tip displacement of 35 mm is reached for a charge transfer of 79.6 $mAhg^{-1}$. The specimen here has average layer thicknesses: carbon fiber 53.4 μm and separator 21.0 μm.

The expansion/contraction strains are proportional to the change in charge (ΔQ) in each of the carbon fiber layers through

$$\varepsilon^{+} = \beta \cdot \Delta Q \text{ and } \varepsilon^{-} = -\beta \cdot \Delta Q, \quad [1]$$

where β is an expansion coefficient. This was calculated as being $\beta = 2.6 \times 10^{-5}$ $g(mAh)^{-1}$ (*SI Appendix*, Fig. S2) measured using a previously described methodology (22). Thus, for a ΔQ of 100 $mAhg^{-1}$ the strain in one layer is 0.26% and in the other −0.26%. The separator does not expand or contract during charge and discharge. The expansion strains create a lengthwise constant curvature of the cantilever, which is related geometrically to the cantilever tip displacement. To validate the analytical model the experiments were also analyzed the finite-element method (FEM) assuming linear elastic materials and large displacements (geometrically nonlinear). The expansion coefficient β was implemented as a thermal expansion. These predicted results are compared to an experimentally measured tip displacement and curvature in Fig. 4, where deviations at large charge difference ΔQ are due to the tip touching the vertical wall in the experiment.

The energy consumed in driving the morphing process is an important parameter to consider. Here, the energy consumed is not just the energy input to the system, as the majority of the energy is stored electrochemically and is recovered by running currents in the opposite direction. Only a small amount of the electrical energy put into the system is converted to elastic strain energy with a conversion around 0.05%. The only real losses are those coming from electrochemical losses similar to those in a conventional Li-ion battery. The gravimetric mechanical strain energies are 22 and 27 Jkg^{-1} for the experiments shown in Figs. 3 and 4, respectively. In bending, strains are varying through the thickness of the material, meaning mechanical strain energy from the tension/compression of the carbon fibers is not fully exploited, resulting in seemingly low actuation energies. Linear actuation could be exploited albeit without creating any bending motion. Both carbon fiber layers would be expanded (or contracted) simultaneously using an external lithium source, similar to the activation step. The linear gravimetric mechanical strain energy would then be around 500 Jkg^{-1} similar to previously reported data (16).

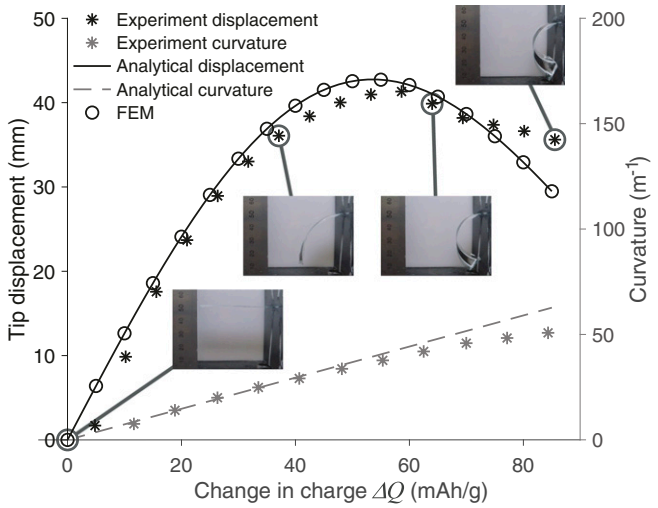

Fig. 4. Comparison between experiment, analytical prediction, and FE model prediction of tip displacement and curvature vs. change in charge for the carbon fiber composite morphing material in a cantilever setup. The specimen here has average layer thicknesses: carbon fiber 40.4 μm and separator 21.3 μm, and a cantilever length of 59 mm.

Discussion

In this paper we have shown it is possible to create a lightweight and stiff material, which is solid-state, morphable with large deformations, exhibits a zero-power hold, and is easy to control at low currents and voltages. It is made from commercial carbon fibers and an SBE using standard manufacturing techniques used in the composite industry, meaning it can be integrated into existing composite structures. Electrochemical actuation means no moving parts are required, enables electrical control at low voltages, and an inherent zero-power hold.

A limitation is that the actuation rate is low, as with any other actuation that exploits ion insertion, since diffusion in solids is generally a slow process. Rate can be improved by increasing the ionic conductivity of the SBE, however it is limited by the ionic conductivities of state-of-the-art Li-ion battery electrolytes. Decreasing layer thicknesses and carbon fiber diameter would also increase morphing rate, as the rate of ion transfer is inversely proportional to the layer thicknesses and inversely proportional to the square of the carbon fiber diameter (30). However, such geometry improvements are limited by the ionic conductivity of the SBE. With these system improvements it is realistic to consider a rate increase of around 10 times. Although this would still constitute comparably slow morphing, there are applications where this is required and even advantageous, such as the trimming of aerodynamic surfaces for steady-state conditions in aircraft and wind turbines, and the deployment of satellite booms in space.

Another limitation is that this morphing composite material is not yet operable in an ambient environment due to the inserted Li and presence of solvents, but this can be remedied by a suitable outer barrier such as layers of ultrathin glass (31).

The concept has potential for future development by tailoring for different applications. For example, the scale of the material could be adjusted, with the lower limit being the size of two single carbon fibers, which could be on the nanoscale. Larger structures could be conceived by adding more and thicker layers of carbon fiber, albeit at the expense of morphing rate. Different modes of morphing such as twisting and rolling deformations could be envisaged by altering the carbon fiber layer orientations. Differing layups would result in trade-offs between material stiffness, magnitude of deformation, mode of deformation, and actuation frequency. This technology could also be combined with a positive electrode layer which would allow the material to inherently store the electrochemical energy required for morphing.

Conclusions

In summary, an electrically controlled solid-state morphing composite material has been manufactured and tested. It is capable of producing large deformations and holding them with no additional power, albeit at low rates. The material is lightweight and has a stiffness higher than aluminum. It consists of two layers of commercial carbon fiber and a separator layer embedded in a structural battery electrolyte. The carbon fibers expand and contract using lithium-ion insertion/extraction at low voltages leading to an overall bending motion. A proof-of-concept morphing material has been presented in a cantilever setup. Analytical modeling shows good correlation with experiments. In conclusion, the composite material presented here shows considerable promise to become a viable alternative for creating stiff solid-state morphing materials.

Experimental

Materials Used. Carbon fibers of the type T800SC-12K-50C manufactured by Toray Composite Materials America, Inc. were used (density 1,800 kgm^{-3}) (32). The carbon fiber tow was spread by Oxeon AB to an approximate width of 10 mm in order to make thin layers. The SBE consists of Bisphenol A ethoxylate dimethacrylate (BAED), M = 364.43 gmol^{-1}, propylene carbonate (99% anhydrous) (PC), ethylene carbonate (99% anhydrous) (EC), lithium trifluoromethanesulfonate (LiTFS) (96%), and 2,2′-Azobis(2-methylpropionitrile) (AIBN), all were supplied by Sigma-Aldrich. The resulting cured SBE has a measured density of 1,100 kgm^{-3}. The separator is a layer of Freudenberg FS 3011–23 (areal weight 0.033 kgm^{-2}) (33). Current collectors were made from copper (17 μm, 99.95% purity) and nickel foil (15 μm, 99.95% purity). Lithium metal foil (0.38 mm, 99.9% purity, Sigma-Aldrich), Whatman GF/A (260-μm) glass fiber paper, and pouch cell bags (PET/Al/PE from Skultuna Flexible) were used during the activation process. DeltaPreg AX003 epoxy adhesive was used to attach the tabs during expansion measurements. All materials were used as received.

Manufacturing. The manufacturing of the composite material was made by stacking of dry layers. First a layer of carbon fiber was laid onto a glass plate mold. A ceramic separator (Freudenberg FS 3011–23) was used as the separator layer, followed by the second layer of carbon fiber. Current collectors on the carbon fiber layers were made from copper foil, and were adhered with Electrolube silver conductive paint. The stack was sealed with vacuum sealing film and dried for 12 h in vacuum at 60 °C before being inserted into dry argon atmosphere (<2 ppm H_2O, <2 ppm O_2). The SBE was prepared in the same argon atmosphere with 60.2 wt % BAED, 0.6 wt % AIBN, and 39.2 wt % liquid electrolyte, which is made from 1.0 M LiTFS in EC:PC 1:1 wt/wt. Vacuum-assisted infusion was used in order to impregnate the SBE into the layup which was then cured at 90 °C for 45 min. The resulting material density of 1,600 kgm^{-3} is based on the constituent densities and their volume fractions.

Activation Process. The activation was done by electrochemically charging and discharging of the carbon layers against Li metal. Nickel current collectors were used to contact the Li metal foils. Electrical insulation between the carbon fiber layers and the Li metal foils was ensured by layers of Whatman GF/A (260-μm) glass fiber paper (Fig. 2*D*). The glass fiber papers were saturated with the liquid electrolyte part of the SBE (1.0 M LiTFS in EC:PC 1:1 wt/wt) for ion conduction. The carbon fibers were electrochemically charged and discharged between 0.002 and 1.5 V vs. Li/Li^+ for about 10 cycles, with a constant current of 18.6 mA per gram of carbon fibers followed by a short potentiostatic step, using a Biologic VSP potentiostat. The current corresponds to a charging time of ∼9.5 h and all cycling was carried out at a temperature of 25 ± 1 °C. The cycling was stopped at ∼50% of the last full cycle charge (*SI Appendix*, Fig. S1), corresponding to 0.85 V vs. Li/Li^+.

Expansion Measurements. The expansion coefficient β for the same carbon fiber and electrolyte as used in the morphing experiments was obtained using the following experimental setup. Glass fiber tabs were attached to single carbon fiber tows using DeltaPreg AX003 epoxy adhesive to provide a means of gripping the fibers in a tensile tester. First, tabbed carbon fiber specimens were tested in tension to obtain the axial stiffness of the tow, giving a value of 1,025 Nmm^{-1}. Next, tabbed carbon fiber specimens were placed in a half-cell setup in a pouch bag with Li metal as the common counter and reference electrode, and a glass fiber paper soaked with electrolyte as a separator. The pouch-cell specimen was mounted in a Shimadzu AGS-X 5kN tensile tester and a

constant strain was applied. The pouch-cell specimen was allowed to relax for 3 h, in order to minimize the load contribution of the viscoelastic pouch bag material. A constant current was applied between the carbon fibers and the Li metal using a Biologic VSP potentiostat in order to charge and discharge the carbon fibers. During charge the carbon fibers expand, resulting in a load drop, and the opposite occurs during discharge. These are correlated to axial expansions/contractions of the carbon fibers through the measured axial stiffness of the tow, since the carbon fiber stiffness remains constant with charge (22). A typical strain per unit charge ratio of $\beta = 2.6 \times 10^{-5}$ g(mAh)$^{-1}$ was measured (*SI Appendix*, Fig. S2).

Actuation Experiment Details. After activation, the pouch was opened in a dry argon atmosphere, with a temperature around 25 °C. The composite material was removed and encapsulated in a low-density polyethylene film with thickness 15 μm. This was clamped in a rig forming a cantilever structure and the copper collectors connected to a Biologic SP-50 potentiostat as a current source. Depending on desired morphing rate, constant currents ranging from 14 to 45 mAhg^{-1} were applied, charging one carbon fiber layer while discharging the other until the potential between the carbon fiber layers reached 1.5 V. The system was then relaxed with a zero-current hold for 60 min. Next, the current was reversed until reaching −1.5 V, followed by 60-min relax time and so on. Deflections were measured at the tip of the cantilever from the time-lapse video obtained using a GoPro Hero4 Session camera. Displacements were acquired using image tracking provided by MATLAB's Image Processing Toolbox. Curvatures were measured from video snapshots using MATLAB image processing and least-square fit of circles to image data points. An example of an actuation experiment video is shown in Movie S1.

Mechanical Characterization. Scanning electron microscope (SEM) imaging was conducted using a Zeiss Leo Ultra 55 field-emission gun SEM at 5-kV acceleration voltage. Prior to imaging all samples were soaked in water for one full day to remove the liquid component of the SBE, dried overnight at 60 °C, and sputter coated with Pt/Pd using an Emitech K500X sputter coater. Cut surfaces were obtained using a scalpel. An example image is shown in Fig. 1*A*. Layer thicknesses of the composite material were measured using an Olympus BX53M light microscope with Olympus Stream Basic (v2.3.3) software, from cut and potted samples, polished to obtain a smooth surface. An example image is shown in Fig. 1*B*. These layer thicknesses were used to calculate the fiber volume fraction of the carbon fiber layers v_f, knowing the tow count [12,000 fibrils (32)] and the carbon fiber diameter (5 μm) (32). The longitudinal elastic modulus E_{cf} of the carbon fiber layers was calculated using the rule of mixtures (34)

$$E_{cf} = E_f v_f + E_m(1 - v_f), \quad [2]$$

where E_f is the elastic modulus of the fibers (294 GPa) (32) and E_m is the elastic modulus of the SBE [0.4 GPa (25)]. The layer thicknesses of the carbon fiber t_{cf} and separator t_s, as well as the longitudinal elastic moduli of the carbon fiber layers are given in *SI Appendix*, Table S1.

Tension tests were performed on the composite material including the two carbon fiber layers and the separator. The size of the specimen was 10 mm wide and 15 mm long. These were performed in an Instron 5567 tensile tester with a 500-N load cell, under a fixed displacement rate of 0.1 mm min^{-1}. The strain was measured using an optical strain mapping system, GOM Aramis. The experimental longitudinal stiffness of the composite material A is calculated as the linear slope of the load–strain curve by

$$A = P/\varepsilon, \quad [3]$$

where P is the load per unit width and ε the measured strain. This is compared to the theoretically predicted longitudinal stiffness defined by

$$A = 2t_{cf}E_{cf} + t_sE_s, \quad [4]$$

assuming an elastic modulus of the separator layer (E_s = 1 GPa). The homogenized longitudinal in-plane elastic modulus of the composite material (E_{mat}) is given by

$$E_{mat} = \frac{A}{2t_{cf} + t_s}. \quad [5]$$

Both the experimental and the theoretically predicted stiffnesses are given in *SI Appendix*, Table S2.

Bending tests were performed in the fiber direction using an Instron 5567 testing machine in a three-point bending setup using specimen width of 10 mm and supported length L of 12 mm and a fixed displacement rate of 1 mm min^{-1}. The experimentally measured bending stiffness D is given by the load–displacement relationship as

$$D = \frac{PL^3}{48\delta}, \quad [6]$$

where δ is the midpoint displacement and P the load per unit width. This is compared to the theoretically predicted bending stiffness given by

$$D = \frac{2}{3}E_{cf}\left(\left(t_{cf} + \frac{t_s}{2}\right)^3 - \left(\frac{t_s}{2}\right)^3\right) + \frac{E_s t_s^3}{12}. \quad [7]$$

The theoretical and experimentally measured stiffness values are given in *SI Appendix*, Table S2.

Modeling of Morphing Behavior. The deflection of the cantilever was analytically predicted using the expansion strains of the two carbon fiber electrode layers. A schematic representation of the composite material and its internal expansion strains is shown in *SI Appendix*, Fig. S3. Herein we use that the expansion strain $\varepsilon^+ = -\varepsilon^-$ and that the strain is proportional to the change in charge, ΔQ in the carbon fibers through Eq. **1**. These expansion strains correspond to a constant bending moment M per unit width calculated using classical lamination theory (34):

$$M = \frac{E_{cf}}{2}\left[\left(t_{cf} + \frac{t_s}{2}\right)^2 - \left(\frac{t_s}{2}\right)^2\right](\varepsilon^+ - \varepsilon^-). \quad [8]$$

The lengthwise constant curvature is given by

$$\kappa = \frac{M}{D}. \quad [9]$$

Since the displacements are large, the cantilever tip displacement cannot be calculated from linear beam theory. The expansion strains cause the cantilever to bend with lengthwise constant curvature, forming a circle segment with an arc length equal to the cantilever length L and curvature κ. With a radius of curvature $R = 1/\kappa$ the circle segment angle is $\theta = \kappa L$. Geometry gives that $\cos\theta = (R - w)/R$ and thus the cantilever tip displacement w is

$$w = \frac{1}{\kappa}(1 - \cos\kappa L). \quad [10]$$

The total strains at the top and bottom of each carbon fiber layer are calculated as

$$\varepsilon_{top}^{tot} = \kappa\left(t_{cf} + \frac{t_s}{2}\right), \varepsilon_{bottom}^{tot} = \kappa\frac{t_s}{2}, \quad [11]$$

and vary linearly within the layer. The mechanical strain is the total strain minus the expansion strain ($\varepsilon^{mech} = \varepsilon^{tot} - \varepsilon^{expansion}$) and the stress in the carbon fiber layers is then $\sigma_{cf} = E_{cf}\,\varepsilon^{mech}$. The strain energy due to bending is calculated as

$$U_{se} = \frac{1}{2}\int \sigma\varepsilon dV = \int_0^{t_c}\frac{\sigma_{cf}^2}{E_{cf}}dz \cdot L \cdot W = \frac{1}{E_{cf}}\left[\sigma_{cf,top}^2 t_c + \sigma_{cf,top}kt_c^2 + k^2\frac{t_{cf}^3}{3}\right] \cdot L \cdot W, \quad [12]$$

where $k = (\sigma_{cf,bottom} - \sigma_{cf,top})/2$, L is the beam length, and W is the beam width. The contribution from the separator is neglected, having low elastic modulus and subjected to low mechanical strains.

To validate the analytical model the cantilever was also modeled in the FE code ABAQUS (35) using four-noded shell elements of the type S4R consisting of three orthotropic layers corresponding to the two carbon fiber layers and the separator. The materials were linear elastic but the analysis accounted for large displacements (geometrically nonlinear) and applying a temperature change to the two carbon fiber layers. The temperature was correlated to ΔQ of the carbon fiber layers such that 0 °C corresponded to the initial condition (both carbon fiber layers have the same state of charge) and 100 °C to the maximum change in charge (positive in one layer and negative in the other).

The total electrical energy U_{elec} in one cycle going from zero displacement to maximum displacement in the experiments was calculated from (e.g., the potential curve in Fig. 3)

$$U_{elec} = I\int_0^T V dt, \quad [14]$$

where I is the applied constant current, V the electrical potential between the carbon fiber layers as function of time, and T the time at maximum displacement.

The conversion from electrical to mechanical energy in the cantilever is

$$conversion = \frac{U_{se}}{U_{elec}}. \quad [15]$$

Data Availability. The raw data for Figs. 3 and 4 and *SI Appendix*, Figs. S1 and S2 and Tables S1 and S2 are available at https://doi.org/10.17632/4zky6h8w3v.1.

ACKNOWLEDGMENTS. The authors would like to acknowledge Anton Shipsha for help in building the FE model, Kevin Geiger for assistance with the initial experiments, and Oxeon AB for supplying spread tow carbon fibers. The Swedish research group Kombatt is acknowledged for its synergism throughout this work. This work was supported by the Swedish Research Council, Projects 2017-03898 and 621-2014-4577, the strategic innovation program LIGHTer (funding provided by Vinnova, the Swedish Energy Agency and Formas), H2020 Clean Sky II Project 738085, and by the Air Force Office of Scientific Research under Award FA9550-17-1-0244.

1. J. E. Huber, N. A. Fleck, M. F. Ashby, The selection of mechanical actuators based on performance indices. *Proc. R. Soc. London, Ser. A* **453**, 2185–2205 (1997).
2. P. Portela, P. Camanho, P. Weaver, I. Bond, Analysis of morphing, multi stable structures actuated by piezoelectric patches. *Comput. Struc.* **86**, 347–356 (2008).
3. J. N. Reddy, On laminated composite plates with integrated sensors and actuators. *Eng. Struct.* **21**, 568–593 (1999).
4. M. Sunar, S. S. Rao, Recent advances in sensing and control of flexible structures via piezoelectric materials technology. *Appl. Mech. Rev.* **52**, 1–16 (1999).
5. L. Kong, W. Chen, Carbon nanotube and graphene-based bioinspired electrochemical actuators. *Adv. Mater.* **26**, 1025–1043 (2014).
6. S. Mehraeen, S. A. Gürsel, M. Papila, F. Ç. Cebeci, Investigation of electrochemical actuation by polyaniline nanofibers. *Smart Mater. Struct.* **26**, 095021 (2017).
7. S. Liu *et al*., High electromechanical response of ionic polymer actuators with controlled-morphology aligned carbon nanotube/nafion nanocomposite electrodes. *Adv. Funct. Mater.* **20**, 3266–3271 (2010).
8. O. Kim, T. J. Shin, M. J. Park, Fast low-voltage electroactive actuators using nanostructured polymer electrolytes. *Nat. Commun.* **4**, 2208 (2013).
9. J. Liang *et al*., Electromechanical actuators based on Graphene and Graphene/Fe3O4 hybrid paper. *Adv. Funct. Mater.* **21**, 3778–3784 (2011).
10. R. H. Baughman *et al*., Carbon nanotube actuators. *Science* **284**, 1340–1344 (1999).
11. G. Gu *et al*., V2O5 nanofibre sheet actuators. *Nat. Mater.* **2**, 316–319 (2003).
12. G. Wu *et al*., Graphitic carbon nitride nanosheet electrode-based high-performance ionic actuator. *Nat. Commun.* **6**, 7258 (2015).
13. S. Barbarino, E. I. Saavedra Flores, R. M. Ajaj, I. Dayyani, M. I. Friswell, A review on shape memory alloys with applications to morphing aircraft. *Smart Mater. Struct.* **23**, 063001 (2014).
14. C. Massey, G. McKnight, W. Barvosa-Carter, P. Liu, "Reversible work by electrochemical intercalation of graphitic materials" in *Proceedings of SPIE Smart Structures and Materials 2005: Electroactive Polymer Actuators and Devices (EAPAD)* (International Society for Optics and Photonics, Bellingham, WA, 2005), vol. 5759.
15. T. E. Chin, U. Rhyner, Y. Koyama, S. R. Hall, Y.-M. Chiang, Lithium rechargeable batteries as electromechanical actuators. *Electrochem. Solid-State Lett.* **9**, A134–A138 (2006).
16. Y. Koyama *et al*., Harnessing the actuation potential of solid-state intercalation compounds. *Adv. Funct. Mater.* **16**, 492–498 (2006).
17. H. Zhang, P. S. Grant, An electrochemical microactuator based on highly textured LiCoO2. *Sens. Actuators B Chem.* **176**, 52–57 (2013).
18. D. J. Johnson, Structural-property relationships in carbon fibres. *J. Phys. D Appl. Phys.* **20**, 286–291 (1987).
19. R. Kanno, Y. Takeda, T. Ichikawa, K. Nakanishi, O. Yamamoto, Carbon as negative electrodes in lithium secondary cells. *J. Power Sources* **26**, 535–543 (1989).
20. J. Hagberg, S. Leijonmarck, G. Lindbergh, High precision coulometry of commercial PAN-based carbon fibers as electrodes in structural batteries. *J. Electrochem. Soc.* **163**, A1790–A1797 (2016).
21. H. Kawaura *et al*., Operando measurement of solid electrolyte interphase formation at working electrode of Li-ion battery by time-slicing neutron reflectometry. *ACS Appl. Mater. Interfaces* **8**, 9540–9544 (2016).
22. E. Jacques, M. Hellqvist Kjell, D. Zenkert, G. Lindbergh, M. Behm, Expansion of carbon fibres induced by lithium intercalation for structural electrode applications. *Carbon* **59**, 246–254 (2013).
23. E. Jacques *et al*., Impact of electrochemical cycling on the tensile properties of carbon fibres for structural lithium-ion composite batteries. *Compos. Sci. Technol.* **72**, 792–798 (2012).
24. Z. Wu *et al*., Utmost limits of various solid electrolyte in all-solid state lithium batteries: A critical review. *Renew. Sustain. Energy Rev.* **109**, 367–385 (2019).
25. N. Ihrner, W. Johannisson, F. Sieland, D. Zenkert, M. Johansson, Structural lithium ion battery electrolytes via reaction induced phase-separation. *J. Mater. Chem. A* **5**, 25652–25659 (2017).
26. W. Johannisson *et al*., Multifunctional performance of a carbon fiber UD lamina electrode for structural batteries. *Compos. Sci. Technol.* **168**, 81–87 (2018).
27. L. M. Schneider, N. Ihrner, D. Zenkert, M. Johansson, Bicontinuous electrolytes via thermally initiated polymerization for structural lithium ion batteries. *ACS Appl. Energy Mater.* **2**, 4362–4369 (2019).
28. G. Alici, N. N. Huynh, Predicting force output of trilayer polymer actuators. *Sens. Actuators A Phys.* **132**, 616–625 (2006).
29. S. Timoshenko, Analysis of bi-metal thermostats. *J. Opt. Soc. Am.* **11**, 233–255 (1925).
30. J. Newman, K. E. Thomas-Alyea, *Electrochemical Systems* (Wiley, ed. 3, 2012).
31. A. Sepúlveda, J. Speulmanns, P. M. Vereecken, Bending impact on the performance of a flexible $Li_4Ti_5O_{12}$-based all-solid-state thin-film battery. *Sci. Technol. Adv. Mater.* **19**, 454–464 (2018).
32. Toray Composite Materials America Inc., T800S intermediate modulus carbon fiber. https://www.toraycma.com/file_viewer.php?id=5126. Accessed 2 September 2019.
33. Freudenberg Performance Materials, Lithium-ion battery separator. https://www.freudenberg-pm.com/-/media/Files/separators,-d-,freudenbergpm,-d-,com/LI_Ion%20Overview%20April%202018%20PRELIMINARY.PDF. Accessed 2 September 2019.
34. I. M. Daniel, O. Ishai, *Engineering Mechanics of Composites* (Oxford University Press, New York, 1994).
35. M. Smith, ABAQUS/Standard User's Manual (Version 6.9, Simulia, Providence, RI, 2009).